THE JOURNAL OF PHYSICAL CHEMISTRY B

Article

pubs.acs.org/JPCB

Dynamics of Biological Water: Insights from Molecular Modeling of Light Scattering in Aqueous Trehalose Solutions

Laura Lupi,*[,†] Lucia Comez,[†,‡] Marco Paolantoni,[§] Daniele Fioretto,[†,∥] and Branka M. Ladanyi[⊥]

[†]Dipartimento di Fisica, Università degli Studi di Perugia, Via Pascoli, I-06123 Perugia, Italy

[‡]IOM-CNR c/o Dipartimento di Fisica, Università di Perugia, Via Pascoli, I-06123, Perugia, Italy

[§]Dipartimento di Chimica, Università di Perugia, via Elce di Sotto, I-06123 Perugia, Italy

[∥]Centro di Eccellenza sui Materiali Innovativi Nanostrutturati (CEMIN), Università of Perugia, via Elce di Sotto 8, 06123 Perugia, Italy

[⊥]Department of Chemistry, Colorado State University, Fort Collins, Colorado 80523-1872, United States

ABSTRACT: Extended depolarized light scattering (EDLS) measurements have been recently employed to investigate the dynamics of water solvating biological molecules, giving evidence of the presence of two different dynamical regimes among water molecules. An interpretation of EDLS has been proposed that provides an independent estimate of the retardation factor of slowdown with respect to fast water molecules and of the number of solvent molecules affected by this slowing down. Nevertheless this measure is an inherently complex one, due to the collective nature of the physical property probed. In the present work a molecular dynamics (MD) approach has been used to more deeply understand experimental results. Time correlation functions of the collective polarizability anisotropy have been calculated for the prototype disaccharide trehalose in aqueous solutions as a function of concentration. The unique capability of MD to disentangle the contributions to the dynamics arising from solute, solvent, and cross terms between the two allowed us to check the reliability of an interpretation that assumes a spectral separation of water and sugar dynamics, as well as to highlight the very presence of two distinct relaxation processes in water. The two processes have been attributed to the dynamics of bulk and hydration water, respectively. A retardation factor of ∼5 and concentration dependent hydration numbers have been observed, in good agreement with experimental results [Paolantoni, M.; et al. *J. Phys. Chem. B* **2009**, *113*, 7874−7878].

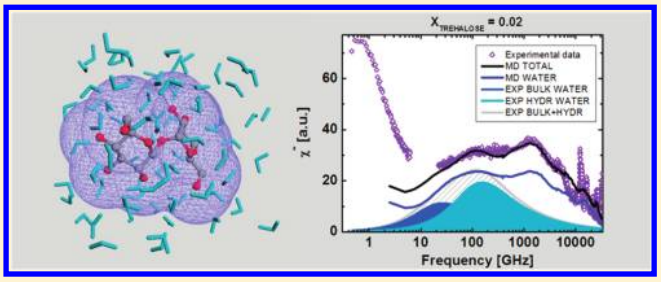

I. INTRODUCTION

Water molecules located at the interface of biological molecules such as proteins and DNA play a crucial role in controlling the structure, function, and reactivity of these systems. For this reason, the characterization of water molecules at the interface is essential for the comprehension of many biological processes and has received increasing attention in the past few years. Significant structural and dynamical differences have been pointed out between water molecules in bulk liquid and those located within the hydration shell of a biomolecule, which are sometime referred to as biological water.[1−3] Disentangling the contribution of hydration from bulk water and from that of the solute is not an easy experimental task, especially considering that the relevant dynamical processes cover wide frequency ranges.

Generally the dynamics of water close to a hydrophilic interface is found to slow down when compared to bulk liquid water, but the degree of the induced retardation and the spatial extent of this effect are strongly debated in the current literature. Relative dynamical retardation factors going from factors of one to hundreds and even larger have been reported depending on the experimental technique and interpretation.[2,4,5] Molecular understanding of these phenomena is not trivial also considering that biological interfaces are intrinsically heterogeneous either from a chemical or a topological point of view. In this regard carbohydrate aqueous solutions can be used as relatively simple hydrophilic systems useful to investigate the modification imposed by an essentially homogeneous hydrogen bonding solute to the structure and dynamics of water molecules in the hydration layer, thus providing an insight into the hydration properties of more complex biological systems, where hydrogen bond interactions must be relevant. Moreover, carbohydrates are per se very interesting for the role they play in a number of biological processes. In nature there are organisms that can suffer extreme desiccation, entering in a state of suspended life, also called anhydrobiosis. It has been observed that this desiccation tolerance in certain living organisms (most of plant seeds, many micro-organisms such as bakers' yeast, and also certain invertebrates) is associated with the production of a significant amount of sugar, which is,

Received: February 29, 2012
Revised: May 28, 2012
Published: May 31, 2012

   dx.doi.org/10.1021/jp301988f | *J. Phys. Chem. B* 2012, 116, 7499−7508

for this reason, thought to be a natural protectant against desiccation damage.[6−8] Moreover, the effectiveness of disaccharides in anhydrobiosis processes has been exploited as an alternative technology to cryoconservation and lyophilization as well, allowing preservation of biological molecules at room temperature.

Among sugars, trehalose (α-D-glucopyranosyl-α-D-glucopyranoside) is known to possess the most effective bioprotective capability;[9] its properties have been known for more than two decades and are still a matter of extensive interest. Different hypotheses have been proposed to explain the stabilizing effect of carbohydrates in general.[7,10−13] However the actual molecular mechanism underlying their strong conservative capability is still unclear. The evidence that one can infer from all of the proposed and widely investigated effects is that they all involve the interrelation between carbohydrates and surrounding water molecules. In this context it appears evident that a deeper comprehension of the role played by water−sugar interaction is fundamental.

A large amount of theoretical and experimental work has been devoted to the study of the dynamical and structural properties of aqueous solutions of carbohydrates in the past two decades. General consensus is found on the presence of two distinct populations of water molecules in carbohydrate solutions.[14,15] Furthermore, experiments and simulations all agree in reporting lower translational and rotational mobility of hydration water around carbohydrates.[16−25] Several molecular dynamics (MD) studies have pointed out the role played by water−water and sugar−water H-bonds and have identified the formation of longer-lived carbohydrate−water H-bonds with respect to the shorter-lived water−water H-bonds to be the main reason for the slow dynamics of hydration water molecules.[18,22,23] However, it has been very challenging to provide experimental evidence to support this finding. The spatial extent of the dynamical perturbation imposed by carbohydrates on the surrounding water molecules,[18−20,26] the perturbation of the water tetrahedral coordination compared to neat water, and the number and stability of H bonds between water and sugars have been intensively investigated.[22,23,27,28] However, agreement does not yet exist regarding the extent of retardation in the relaxation of water molecules in the solvation shells and the spatial extent of the perturbation. Thus a clarification of these issues is needed.

Very recently the extended depolarized light scattering (EDLS) technique has been shown to be a suitable tool to investigate the dynamics of aqueous solution of biological molecules, from carbohydrates[26,29−31] to peptides[32] to more complex molecules such as proteins,[33] providing the opportunity to follow this dynamics over a very wide frequency range, including the solute rotational diffusion, the relaxation of water, and the intermolecular bending and stretching of water molecules. An interpretation of EDLS spectra has been proposed that offers the possibility of an independent estimate of both the retardation factor of hydration with respect to bulk water molecules and of the number of water molecules slowed down.[26,31] Insights into hydration properties of biorelevant molecules can also be obtained by time-resolved optical Kerr effect (OKE) experiments which represent the time-domain counterpart of depolarized light scattering (DLS).[34,35] Because the molecular property probed by EDLS and OKE is a collective one, namely the fluctuations of macroscopic optical anisotropy, simple interpretation of the experimental spectra in terms of contributions arising from solute and solvent molecules requires a careful theoretical examination. In the present work, MD simulation approach is proposed to address this critical issue, to shed more light on hydration properties of aqueous solutions of carbohydrates, and to determine how many and to what extent are water molecules perturbed by trehalose solute molecules. Time correlation functions (TCFs) of the collective polarizability anisotropy have been calculated for aqueous trehalose solutions as a function of concentration. The unique capability of MD to disentangle the contributions to the dynamics arising from solute, solvent, and cross terms between them allowed us to investigate the reliability of the spectral separation of water and trehalose dynamics, as well as to highlight the very presence of two distinct relaxation processes in water.

In section II, we present the theoretical background for the present MD study. This includes the description of the potential model, system parameters, simulation procedures, definitions of the quantities contributing to the DLS spectrum, and specification of the model used to represent the collective polarizability. Our results are presented and discussed in section III, and our conclusions are summarized in section IV.

II. THEORETICAL BACKGROUND

II.A. Potential Models and Simulation Details. Our MD simulation was carried out using the DL_POLY2.0 package.[36,37] The MD trajectories were generated using the SPC/E potential model for water[38] and the optimized potential for liquid simulation (OPLS) all-atom force field for carbohydrates, developed by Jorgensen et al.,[39] for trehalose. The SPC/E model treats the molecules as nonpolarizable, rigid bodies, interacting via a pairwise sum of site−site interactions involving electrostatic terms between fixed partial charges and Lennard-Jones (LJ) interactions, with a single LJ site on the oxygen atom. Within the all-atom OPLS model, trehalose is represented by 45 interaction sites and modeled as a fully flexible molecule.[39] Bonded interactions include stretching, bending, and torsional potentials. Bond stretching and bending were described by harmonic potentials given by

$$V_{\text{stretch}} = K_{\text{r}}(r - r_{\text{eq}})^2 \tag{1}$$

$$V_{\text{bend}} = K_{\vartheta}(\vartheta - \vartheta_{\text{eq}})^2 \tag{2}$$

where K_{r}, K_{ϑ}, r_{eq}, and ϑ_{eq} are the stretching and bending force constants and the equilibrium bond length and angle, respectively. The torsional potential is described by

$$V_{\text{tor}} = \frac{V_1}{2}[1 + \cos(\varphi)] + \frac{V_2}{2}[1 + \cos(2\varphi)] + \frac{V_3}{2}[1 + \cos(3\varphi)] \tag{3}$$

where ϕ is the dihedral angle and V_1, V_2, and V_3 are the torsional parameters. The nonbonded interactions include Coulombic and Lennard-Jones potentials between atoms separated by at least three bonds within the same trehalose molecule and between atoms on different molecules

$$V_{\text{nb},ij}(r) = \frac{q_i q_j}{4\pi\varepsilon_0 r} + 4\varepsilon_{ij}\left[\left(\frac{\sigma_{ij}}{r}\right)^{12} - \left(\frac{\sigma_{ij}}{r}\right)^{6}\right] \tag{4}$$

where r is the separation distance between atoms i and j, q_i is the value of the partial charge on atom i, and ε_{ij} and σ_{ij} are the LJ energy and length parameter, respectively. For atoms

dx.doi.org/10.1021/jp301988f | J. Phys. Chem. B 2012, 116, 7499−7508

separated by three bonds within a trehalose molecule, the nonbonded interaction is decreased by a factor of 2. The LJ parameters between different types of atoms were calculated using the Lorentz–Berthelot mixing rules[40]

$$\sigma_{ij} = \frac{1}{2}(\sigma_i + \sigma_j) \tag{5}$$

$$\varepsilon_{ij} = \sqrt{\varepsilon_i \varepsilon_j} \tag{6}$$

which give slightly different values for ε_{ij} and σ_{ij} from those obtained using the OPLS combining rules.[39] The OPLS model was chosen for this study because it is a relatively simple, pairwise-additive, potential that has been shown to be accurate for the properties of trehalose–water solutions relevant to the present application.[18,28] Intramolecular distances within water molecules were kept fixed by using the SHAKE iterative procedure.[41] The constraint method was used to integrate the equations of motion of the rigid molecules, in combination with the velocity Verlet algorithm, with a time step of 1 fs. We have considered, in addition to the pure water, aqueous mixtures having trehalose mole fractions of X_{TRE} = 0.004, 0.009, 0.02, and 0.04. The simulations were performed in the microcanonical ensemble with a total number of N = 200–250 molecules placed in a cubic box with periodic boundary conditions. Short-ranged intermolecular interactions were cut off at half the box length, whereas standard Ewald sums with conducting boundaries were used to handle long-range Coulombic forces. Preliminary trajectories of 200 ps in the *NPT* ensemble were first run in order to equilibrate the system at 300 K and 1 atm. Production runs of 2 ns each were then generated in the microcanonical ensemble. TCFs, calculated up to 400 ps, were averaged over tens of uncorrelated runs to improve statistics.

II.B. Light Scattering Response. The response observed in EDLS experiments is related to the relaxation of the polarizability anisotropy of the system and can be described by the time autocorrelation function of an off-diagonal component Π_{xz} of the collective polarizability tensor $\boldsymbol{\Pi}$

$$\Psi(t) = \langle \Pi_{xz}(0)\Pi_{xz}(t)\rangle/\Gamma^2 \tag{7}$$

where Γ^2 represents the depolarized light scattering intensity, i.e., the mean squared polarizability anisotropy, of a noninteracting system containing the same number and types of molecules as the system of interest. It is given by $\Gamma^2 = N\gamma^2/15$, where $\gamma^2 = (x_{TRE}{}^2\langle\gamma_{TRE}{}^2\rangle + x_W{}^2\gamma_W{}^2)$ is the square of the mixture's ideal-gas polarizability anisotropy, with $\gamma_a{}^2 = [(\alpha_{11,a} - \alpha_{22,a})^2 + (\alpha_{11,a} - \alpha_{33,a})^2 + (\alpha_{22,a} - \alpha_{33,a})^2]/2$ and $\alpha_{jj,a}$ the principal polarizability components of a molecule of type a. Trehalose molecules are flexible, so $\gamma_{TRE}{}^2$ needs to be averaged over molecular conformations.

The susceptibility spectra are obtained from molecular dynamics simulations after calculating the OKE nuclear response function[42,43] $R(t)$ defined as

$$R(t) = -\frac{1}{k_B T}\frac{\partial}{\partial t}\Psi(t) \tag{8}$$

where $(k_B T)^{-1}$ is the usual Boltzmann factor. The imaginary part of the susceptibility $\chi''(\omega)$ is obtained as by performing a Fourier–Laplace transform (FT) of $R(t)$

$$\chi''(\omega) \equiv Im[\chi(\omega)] = \int_0^\infty \sin(\omega t)R(t)\,dt \tag{9}$$

that corresponds to the susceptibility obtained from experimental Raman scattered intensity $I_{HV}(\omega)$ according to the relation $\chi''(\omega) = I_{HV}(\omega)/[n_B(\omega) + 1]$, where $n_B(\omega) = 1/[\exp(\hbar\omega/k_B T) - 1]$ is the Bose–Einstein occupation number.[26]

The collective polarizability tensor, Π, for a condensed-phase system composed of N molecules can be expressed as a sum of molecular $\boldsymbol{\Pi}^M$ and induced $\boldsymbol{\Pi}^I$ contributions

$$\boldsymbol{\Pi} = \boldsymbol{\Pi}^M + \boldsymbol{\Pi}^I \tag{10}$$

where the molecular part is simply given by the sum of the intrinsic molecular polarizabilities $\boldsymbol{\alpha}_i$

$$\boldsymbol{\Pi}^M = \sum_{i=1}^{N} \boldsymbol{\alpha}_i \tag{11}$$

The induced contribution, $\boldsymbol{\Pi}^I$, arises from interactions between molecular induced dipoles. It depends on orientational, conformational, and translational degrees of freedom, and it can be interpreted as a dynamical modulation of the polarizabilities. Moreover, for a system of two distinct species of molecules, the total molecular polarizability arises from the sum of the polarizability tensors of the two species; in the case of water–trehalose solution, it can be expressed by

$$\boldsymbol{\Pi}^M = \boldsymbol{\Pi}^{M,W} + \boldsymbol{\Pi}^{M,TRE} \tag{12}$$

whereas the interaction-induced polarizability also includes interactions between the two species

$$\boldsymbol{\Pi}^I = \boldsymbol{\Pi}^{I,W} + \boldsymbol{\Pi}^{I,TRE} + \boldsymbol{\Pi}^{I,W-TRE} \tag{13}$$

Based on eqs 12 and 13, the TCF of the total collective polarizability $\Psi(t) = \Psi^{TOT}(t)$ can be separated into the three terms, $\Psi^W(t)$, $\Psi^{TRE}(t)$, and $\Psi^{W-TRE}(t)$, the first two arising from autocorrelations of water and trehalose anisotropic polarizibilities, $\Pi_{xz}^W = \Pi_{xz}^{M,W} + \Pi_{xz}^{I,W}$ and $\Pi_{xz}^{TRE} = \Pi_{xz}^{M,TRE} + \Pi_{xz}^{I,TRE}$, whereas the third one arises from cross-correlations between Π_{xz}^W and Π_{xz}^{TRE} as well as from terms that include the interspecies interaction-induced anisotropic polarizability, $\Pi_{xz}^{I,W-TRE}$. Moreover, based on eq 10, $\Psi^W(t)$, $\Psi^{TRE}(t)$, and $\Psi^{W-TRE}(t)$ can each be separated into three terms, $\Psi^{MM}(t)$, $\Psi^{II}(t)$ and $\Psi^{MI}(t)$, arising from the autocorrelations of molecular and induced polarizabilities and the cross term between them.

II.C. Molecular Polarizability. The water intrinsic molecular polarizability tensor employed in the calculations was taken from ab initio quantum chemical calculations at the MP3/6-31+G(2df,p) level.[44]

The polarizability for water, calculated by Skaf and Vechi,[44] is more anisotropic than the nearly isotropic gas phase polarizability tensor obtained by Murphy[45] in 1977 and is more successful[46] in reproducing the librational features found in the OKE response of liquid water.[47] Hence, we chose to use in our calculations the more anisotropic polarizability tensor for water computed by Skaf and Vechi.

The calculation of the molecular polarizability of trehalose solute was performed using the Thole model[48] with parameters given by van Duijnen and Swart.[49] In this model, a dipole moment $\boldsymbol{\mu}_p$ in atom p is induced by the applied field $\mathbf{E}$ and by the dipoles $\boldsymbol{\mu}_q$ of other atoms within the same molecule

$$\boldsymbol{\mu}_p = \boldsymbol{\alpha}_p[\mathbf{E} - \sum_{q\neq p} \mathbf{T}(\mathbf{r}_{pq})\cdot\boldsymbol{\mu}_q] \tag{14}$$

dx.doi.org/10.1021/jp301988f | J. Phys. Chem. B 2012, 116, 7499–7508

where $\boldsymbol{\alpha}_p$ is the polarizability of atom p, taken as isotropic in the model, and $\mathbf{T}$ is the modified dipole interaction tensor which depends on the interatomic distance vector $\mathbf{r}_{pq}$. Thole considered several functional forms to represent the attenuation of dipolar interactions at short distances in order to avoid the unphysical divergence of the polarization. We use here the form referred to as "linear".[48,49] This form is given by

$$\mathbf{T}(\mathbf{r}) = (\mathbf{1} - 3\hat{\mathbf{r}}\hat{\mathbf{r}})/r^3, \quad r > s$$
$$\mathbf{T}(\mathbf{r}) = [(4v^3 - 3v^4)\mathbf{1} - 3v^4\hat{\mathbf{r}}\hat{\mathbf{r}}]/r^3, \quad r \leq s \tag{15}$$

where $\hat{\mathbf{r}} = \mathbf{r}/r$, $v = r/s$, and s is a distance whose scale is set by the atomic polarizabilities

$$s = 1.7823(\alpha_p\alpha_q)^{1/6} \tag{16}$$

Equation 14 can be written in matrix form

$$\mathbf{RM} = \mathbf{E} \tag{17}$$

where, for an m-atomic molecule, $\mathbf{R}$ is a $3m \times 3m$ "relay" matrix containing 3×3 diagonal blocks of inverse atomic polarizabilities and 3×3 off-diagonal blocks of modified dipole tensors and $\mathbf{M}$ is a $3m$ vector of induced dipoles. The molecular polarizability is obtained by inverting eq 17

$$\mathbf{A} = (\boldsymbol{\alpha}^{-1} + \mathbf{T})^{-1} = \mathbf{R}^{-1} \tag{18}$$

and by summing the 3×3 blocks of matrix $\mathbf{A}$ over atoms

$$\boldsymbol{\alpha} = \sum_{p=1}^{m}\sum_{q=1}^{m}\mathbf{A}_{pq} \tag{19}$$

II.D. Interaction-Induced Polarizability. Since water molecules are small, we represent them as single polarizable sites with the molecular polarizability tensor elements taken from the work of Skaf and Vechi.[44] The induced polarizability for the N_W water molecules is evaluated using the center−center dipole-induced-dipole model (DID) expressed by the molecular counterpart of eq 14, in which the site-induced dipoles and polarizabilities $\boldsymbol{\mu}_p$ and $\boldsymbol{\alpha}_p$ are replaced by molecular induced dipoles and polarizabilities $\boldsymbol{\mu}_i$ and $\boldsymbol{\alpha}_i$ and the intersite distance $\mathbf{r}_{pq}$ by $\mathbf{r}_{ij}$, the distance between the centers of mass of molecules i and j. For fluids of molecules that are not highly polarizable, $\boldsymbol{\mu}_i$ can be evaluated to first order in intermolecular interactions

$$\boldsymbol{\mu}_i = [\boldsymbol{\alpha}_i - \sum_{j\neq i}\boldsymbol{\alpha}_i\cdot\mathbf{T}(\mathbf{r}_{ij})\cdot\boldsymbol{\alpha}_j]\cdot\mathbf{E} \tag{20}$$

giving the following expression for $\boldsymbol{\Pi}^{\mathrm{I,W}}$

$$\boldsymbol{\Pi}^{\mathrm{I,W}} \cong -\sum_{i=1}^{N_W}\sum_{j\neq i}\boldsymbol{\alpha}_i\cdot\mathbf{T}(\mathbf{r}_{ij})\cdot\boldsymbol{\alpha}_j \tag{21}$$

A calculation was performed using MD simulation data for pure liquid water, which demonstrated that $\boldsymbol{\Pi}^{\mathrm{I,W}}$ obtained by an iterative solution the all-orders DID model did not give a noticeably different result from the first-order approximation. The less expensive first-order approach was also employed for the trehalose contributions to interaction-induced polarizability.

A limitation of the center−center DID model is that it treats the polarizability as centered in the center of mass of the molecule. It therefore cannot describe accurately interactions between large polyatomic molecules such as trehalose. A more reasonable approach is to use a site-based model to represent induced trehalose contributions to the interaction-induced polarizability. It is possible to calculate the effective site polarizabilities to use in the intermolecular interaction model from the $3m \times 3m$ (m = 45 for our 45-site model) $\mathbf{A}$ matrix (eq 18)

$$\boldsymbol{\alpha}_p^{\mathrm{eff}} = \sum_{q=1}^{45}\mathbf{A}_{pq} \tag{22}$$

The counterpart of eq 21 for a site−site DID interaction model can be written in terms of effective site polarizabilities

$$\boldsymbol{\Pi}^{\mathrm{I,TRE}} \cong -\sum_{i=1}^{N_{\mathrm{TRE}}}\sum_{j\neq i}\sum_{p=1}^{45}\sum_{q=1}^{45}\boldsymbol{\alpha}_{i,p}^{\mathrm{eff}}\cdot\mathbf{T}(\mathbf{r}_{ij}^{pq})\cdot\boldsymbol{\alpha}_{j,q}^{\mathrm{eff}} \tag{23}$$

where $\boldsymbol{\alpha}_{i,p}^{\mathrm{eff}}$ is the polarizability of the site p on molecule i, and $\mathbf{r}_{ij}^{pq} = \mathbf{r}_{i,p} - \mathbf{r}_{j,q}$ the distance between site p on molecule i and site q on molecule j. This model gives a more realistic representation of the charge distribution of the molecule and is fully consistent with the molecular polarizability calculation.

Finally, the collective polarizability of water-trehalose solutions also includes an induced contribution due to interactions between water and trehalose molecules

$$\boldsymbol{\Pi}^{\mathrm{I,W-TRE}} \cong -\sum_{i=1}^{N_W}\sum_{j=1}^{N_{\mathrm{TRE}}}\sum_{p=1}^{45}\boldsymbol{\alpha}_i\cdot\mathbf{T}(\mathbf{r}_{ij,p})\cdot\boldsymbol{\alpha}_{j,p}^{\mathrm{eff}} + \boldsymbol{\alpha}_{j,p}^{\mathrm{eff}}\cdot\mathbf{T}(\mathbf{r}_{ij,p})\cdot\boldsymbol{\alpha}_i \tag{24}$$

where $\mathbf{r}_{ij,p} = \mathbf{r}_i - \mathbf{r}_{j,q}$ is the distance between the center of water molecule i and site p on trehalose molecule j.

III. RESULTS AND DISCUSSION

The normalized polarizability anisotropy TCFs, $\Psi^{\mathrm{TOT}}(t)/\Psi^{\mathrm{TOT}}(0)$, obtained from simulations for pure water and for trehalose−water solutions at different concentrations at T = 300 K are reported in Figure 1. The calculated TCF of neat water, which is in agreement with that obtained in other studies,[46,50] shows oscillatory features at short time-scales (ca. <0.5 ps) followed by a slower relaxation term centered at ca. 1 ps. From a physical point of view the ultrafast dynamics is related to intermolecular bending, stretching and hindered rotations (librations) of water molecules, whereas the slower

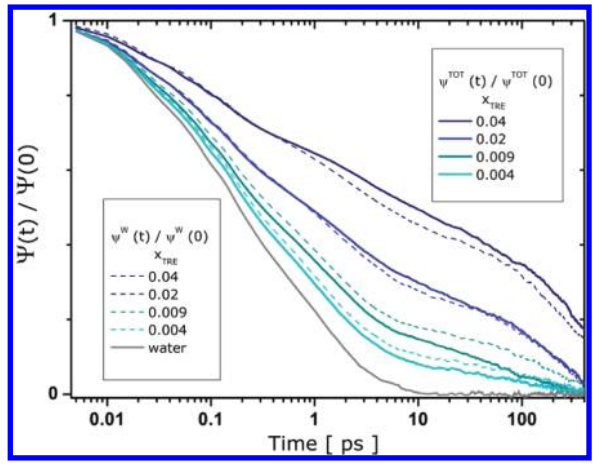

Figure 1. Total polarizability anisotropy time correlation $\Psi^{\mathrm{TOT}}(t)/\Psi^{\mathrm{TOT}}(0)$ of pure water and of water-trehalose solutions at four different mole fractions (continuous line) and the corresponding contributions from water normalized at their initial values $\Psi^{\mathrm{W}}(t)/\Psi^{\mathrm{W}}(0)$ (thinner dashed line).

dx.doi.org/10.1021/jp301988f | J. Phys. Chem. B 2012, 116, 7499−7508

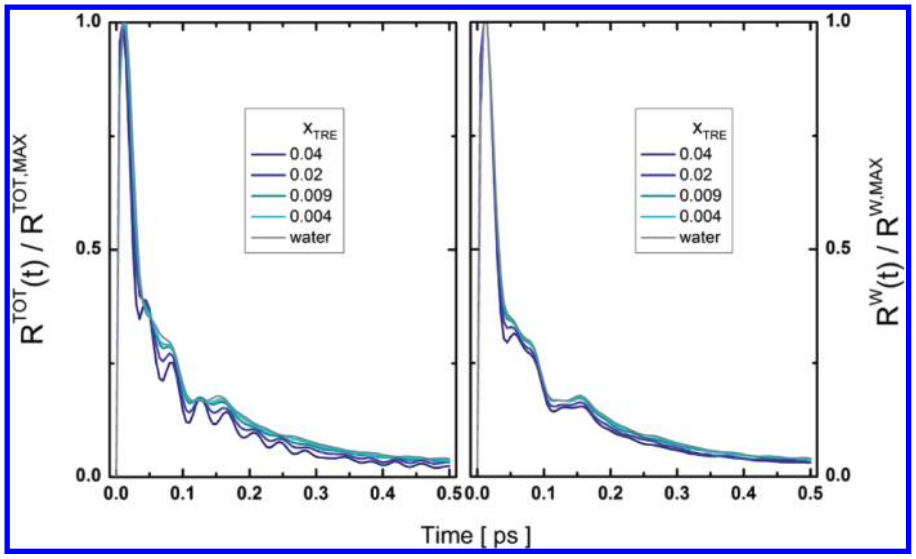

Figure 2. The total nuclear optical Kerr effect (OKE) response function $R^{TOT}(t)$, divided by its maximum value $R^{TOT,MAX}$, of pure water and of water−trehalose solutions (left panel). Pure water and water partial OKE response $R^{W}(t)/R^{W,MAX}$ corresponding to the four different trehalose mole fractions (right panel).

relaxation term can be assigned to a water structural reorganization process connected to the dynamical rearrangement of hydrogen bonds in water.[47,50,51] As shown in Figure 1, the dynamics of the collective polarizability anisotropy of the system is strongly affected by mixing: the overall decay rate exhibits a progressive decrease going from pure water to the highest concentration of sugar.

Figure 1 reports, together with the total TCFs, $\Psi^{TOT}(t)/\Psi^{TOT}(0)$, the partial water contributions normalized by their initial values, $\Psi^{W}(t)/\Psi^{W}(0)$. The comparison emphasizes the similarities of the decay rates of the total and water contributions, suggesting that the relaxation of the system anisotropy is essentially driven by the water contribution alone, which is, then, expected to slow down with increasing trehalose concentration.

To highlight the short time oscillatory behavior, Figure 2 depicts the calculated OKE nuclear response functions (eq 8), $R(t)$, which, in this region, appear very similar at all concentrations (left panel), providing evidence that the solute does not strongly affect the intermolecular dynamics of the system and that the detected slowing down is not related to this ultrafast dynamics. Moreover, the $R(t)$ functions calculated from the water partial contribution $\Psi^{W}(t)$ and reported in the right panel of Figure 2 together with the $R(t)$ function for neat water, show that intermolecular bending, stretching, and librations of water molecules are not modified upon mixing. As a result, these findings indicate that DLS and OKE spectroscopies are suitable to selectively study water properties in sugar aqueous solutions, in spite of the low polarizability anisotropy of water.

To gain more insight into this, separate contributions to the total polarizability anisotropy TCF coming from sugar ($\Psi^{TRE}(t)$), water ($\Psi^{W}(t)$), and cross terms ($\Psi^{W-TRE}(t)$) are calculated and displayed in Figure 3 for the lowest and highest trehalose mole fractions investigated X_{TRE} = 0.004 and 0.04. The trehalose $\Psi^{TRE}(t)$ and the cross $\Psi^{W-TRE}(t)$ terms show a much slower decay rate than the water TCF, $\Psi^{W}(t)$, thus giving a minor contribution to the time evolution of $\Psi^{TOT}(t)$ up to tens of picoseconds. The cross contribution is negative and its decay rate is similar to that of the trehalose term. Going from

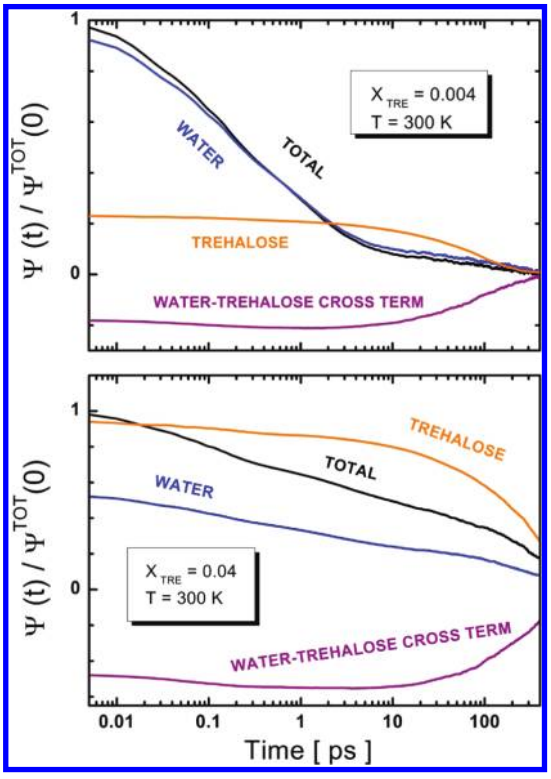

Figure 3. Total polarizability anisotropy TCF $\Psi^{TOT}(t)/\Psi^{TOT}(0)$ (black line) and the corresponding contributions from trehalose (orange line), water (blue line), and trehalose−water cross terms (purple line), for X_{TRE} = 0.004 (top panel) and for X_{TRE} = 0.04 (bottom panel), both at 300 K.

the most dilute to the most concentrated solution we observe that the trehalose and cross contributions grow in magnitude, and that the relaxation rates of these components become progressively slower. As a net result, the behavior of the total relaxation up to tens of picoseconds is dominated by water dynamics at all the concentrations.

It is interesting to note that the presence of a negative cross-term has the effect of lowering the total intensity below the

dx.doi.org/10.1021/jp301988f | J. Phys. Chem. B 2012, 116, 7499−7508

value expected by considering the anisotropic polarizability of the trehalose molecule alone. In this respect the presence of the aqueous medium decreases the intrinsic anisotropy of the sugar and enhances the relative contribution of water, analogous to what has been observed for formamide[50] and contrary to the trend found for the DMSO solute.[44] The decomposition (not shown) of the cross term $\Psi^{W-TRE}(t)$ into constituent components (see eqs 10, 12, and 13) indicates, in addition, that the major negative contributions to this term arise from the correlation between $\Pi_{xz}^{I,W}$ and $\Pi_{xz}^{I,W-TRE}$ and between Π_{xz}^{M-TRE} and $\Pi_{xz}^{I,W-TRE}$, that is, between the water−water and water−trehalose induced polarizabilities, and between the trehalose molecular polarizability and the water-trehalose induction again, thus confirming the view of a reduction of the intrinsic anisotropy, imposed on the sugar by the presence of the aqueous solvent.

It is also possible to investigate the origin of the Raman scattered intensity in terms of the underlying molecular mechanisms. Based on eq 4, both $\Psi^{W}(t)$ and $\Psi^{TRE}(t)$ can be separated into three terms, arising from the autocorrelations of molecular (MM) and induced polarizabilities (II), and the cross term between the two (MI). In Figure 4 the decomposition of water TCFs $\Psi^{W}(t)$ into $\Psi^{W,MM}(t)$, $\Psi^{W,II}(t)$, and $\Psi^{W,MI}(t)$ is shown for water in a X_{TRE} = 0.004 (left panel) and a X_{TRE} = 0.04 (right panel) mole fractions.

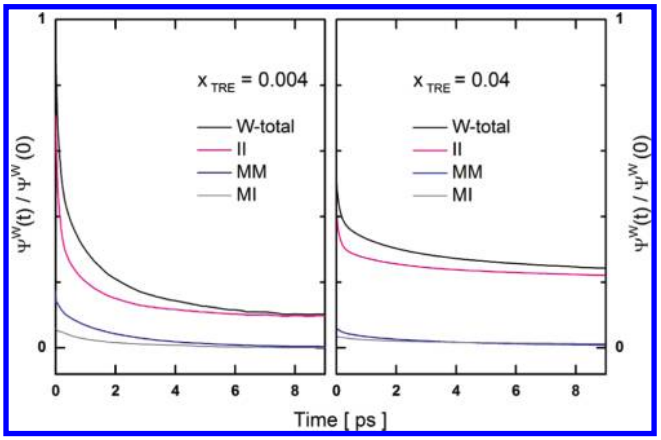

Figure 4. Molecular (MM), interaction-induced (II), and cross (MI) contributions to $\Psi^{W}(t)$ for in trehalose aqueous solutions at X_{TRE} = 0.004 (left panel) and X_{TRE} = 0.04 (right panel).

It can be seen that the major contribution to $\Psi^{W}(t)$ comes from the induced component at both extreme compositions, consistently with what was observed for neat water,[50] indicating that the molecular mechanism underlying water polarizability anisotropy relaxation is dominated by translational dynamics also upon mixing. Moreover, this component, which depends mainly on the intermolecular separation of water molecules, is known to be strongly affected by the relaxation rate of the hydrogen bond network of the mixtures.[50,52] It is also worth mentioning that the $\Psi^{W,MM}(t)$ correlations exhibit the fastest relaxation rate, while $\Psi^{W,II}(t)$ shows the slowest relaxation rate and is the most affected by the retardation. The $\Psi^{W,MI}(t)$ component is positive in the whole time scale displayed. On the contrary, an analogous decomposition (not shown) of $\Psi^{TRE}(t)$ has its major contribution from the molecular $\Psi^{TRE,MM}(t)$ component, which arises from rotational and conformational degrees of freedom of trehalose molecules.

Note that, as has been shown, the advantage of MD with respect to the experiment is the possibility to dissect the TCFs into constituent components. However, to reliably identify the contributions to the experimental signal arising from different molecules and mechanisms as observed from MD, the reproducibility of the experimental data has to be tested. Figure 5 shows the direct comparison between the calculated

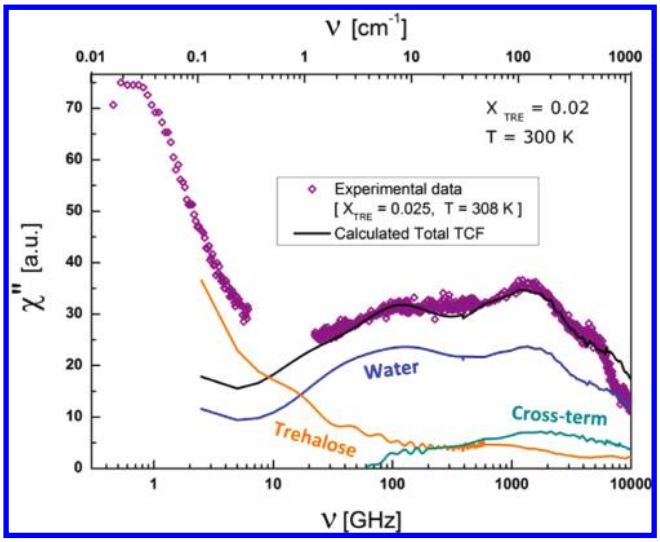

Figure 5. Susceptibility of the X_{TRE} = 0.02 trehalose-water solution at 300 K, as obtained from Fourier transforms of the total polarizability anisotropy time correlation $\Psi^{TOT}(t)$ (black line), and its components: trehalose $\Psi^{TRE}(t)$ (orange line), water $\Psi^{W}(0)$ (blue line), and cross term $\Psi^{TRE-W}(t)$ (dark cyan line). Experimental data (ref 26) are reported for X_{TRE} = 0.025 at 308 K (purple symbols).

total susceptibility (black line) and the experimental spectrum (purple symbols) for trehalose mole fractions of 0.021 at 300 K and 0.025 at 308 K, respectively. EDLS experiments were performed according to the procedure described in the experimental section of ref 26.

The good agreement between computational and experimental results indicates that the force field and the polarizability model used in our simulations are suitable to reproduce the collective polarizability dynamics of trehalose-water solutions. Together with the total susceptibility, Figure 5 shows the separate contributions to the spectra arising from solute, solvent and cross terms. In this representation it is again evident that there is a dynamical separation of water and trehalose contributions. In particular, the spectral region above ca. 10 GHz, very well reproduced by the simulation, can be assigned mainly to water dynamics. Furthermore, it can be observed that there are no relevant solute contributions around 100 GHz, the frequency region associated to the water structural relaxation. Finally, the cross term only slightly affects the higher frequency region related to intermolecular stretching and bending modes of water molecules. It can be seen from the figure that the simulation fails to reproduce the intensity of the experimental susceptibility at very low frequencies. The reason for this minor disagreement might be due to the fact that interaction-induced polarizability is approximated to terms of a first order model. In the case of trehalose, which is more polarizable than water, higher orders in interactions may not be negligible. Also, the two temperatures are slightly different and the trehalose mole fraction in the experiment is larger, which will increase the low-frequency peak intensity. On the other

dx.doi.org/10.1021/jp301988f | J. Phys. Chem. B 2012, 116, 7499−7508

hand, even though the intensity of the long-time decay is not well reproduced by our model, its characteristic time scale is close to the experimental one; the discussion of the long-time decay of total and water contributions will be the subject of a future investigation. We now focus our attention on the dynamics of water solvating trehalose molecules.

To further check the quantitative agreement between simulation and experiment, a fitting procedure of the calculated TCFs, $\Psi^{TOT}(t)$, of pure water and of water trehalose solutions at all concentrations is performed and the results compared to the fitting parameters obtained from experimental data. In the case of pure water, the TCF obtained from our simulation at 300 K has been fitted to a single Kohlrausch–Williams–Watts (KWW) function,[53] with characteristic time and stretching parameter in good agreement with previous simulation results.[52] As trehalose is added to water, the appearance of the additional tail at long times does not allow us to fit the total TCFs, $\Psi^{TOT}(t)$, to a single KWW function. Three different contributions were needed to reproduce the 0.4–400 ps region at all concentrations. Two of these are KWW functions, associated with the relaxation of two populations of water molecules. One corresponds to water molecules outside trehalose solvation shells and exhibits bulk-like dynamics. The other one is associated with water molecules that are slowed down by the presence of the solute (hydration water). Finally, a simple exponential function accounts for the much slower dynamics possibly related to the rotational diffusion of

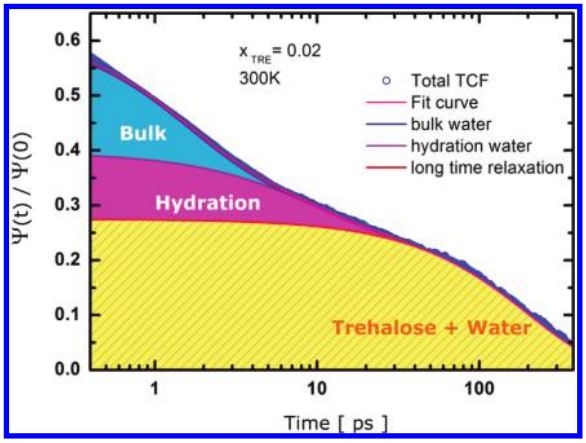

Figure 6. Polarizability anisotropy time correlation function of the X_{TRE} = 0.02 trehalose-water solution at 300 K. The fitting curve (pink line) is also shown together with its components: two Kohlrausch–Williams–Watts functions for the relaxation of bulk and hydration water and a simple exponential function for the long-time decay.

trehalose molecules. Figure 6 shows the goodness of the fit with the model fitting function

$$\Psi^{TOT}(t) = \Delta_{bulk} e^{-(t/\tau_{bulk})^{\beta}} + \Delta_{hydr} e^{-(t/\tau_{hydr})^{\beta}} + \Delta_{long} e^{-t/\tau_{long}} \quad (25)$$

where Δ_{bulk} and Δ_{hydr} are the amplitudes and τ_{bulk} and τ_{hydr} the relaxation times of, respectively, bulk and hydration water molecules, while Δ_{long} and τ_{long} the amplitude and relaxation time of the long time decay. The stretching parameter β of the two KWW functions, used to model the contributions of bulk and hydration water, was fixed to the value obtained for pure water β = 0.6,[26,46,47,54] whereas the relaxation times and amplitudes were left free. The simple exponential function used to describe the long time decay ~20–400 ps, shows a concentration dependent characteristic time of hundreds of picoseconds. The average relaxation times of bulk and hydration water can be obtained from the stretched exponential parameter by the relation

$$\langle \tau \rangle = \frac{\tau_{KWW}}{\beta} \Gamma\left(\frac{1}{\beta}\right) \quad (26)$$

and are shown in Figure 7 as a function of trehalose concentration.

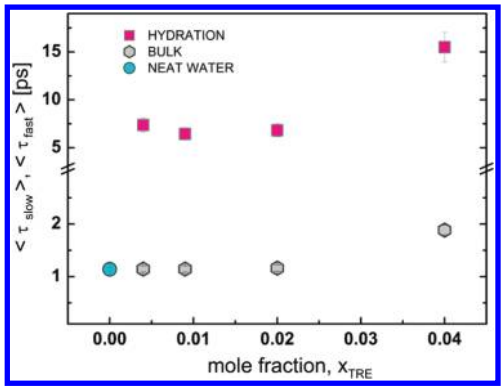

Figure 7. Relaxation times, obtained from the fit of $\Psi^{TOT}(t)$, of bulk and hydration water as functions of trehalose concentration, together with the relaxation time of the simulated pure water (cyan circle).

It can be seen that the faster relaxation time, assigned to a bulk like water dynamics, is similar to that obtained for pure water, ca. 1 ps, at all concentrations, while the slower one, assigned to hydration water, gives a retardation ratio, $\xi = \langle \tau_{hydr} \rangle / \langle \tau_{bulk} \rangle$, between bulk and hydration water molecules of ca. 5, which is comparable to the experimental ratio[26] (Figure 8). A similar fitting procedure can be used to reproduce the

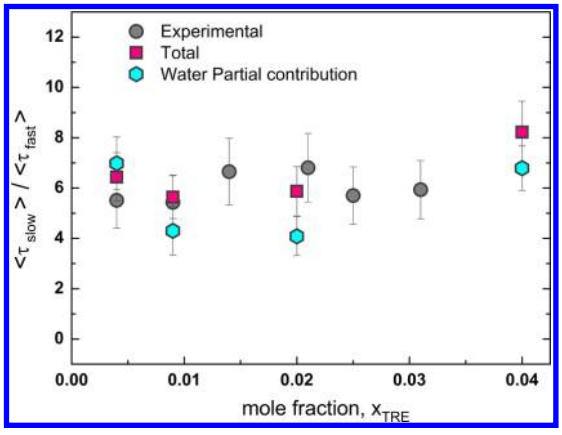

Figure 8. Retardation factor of hydration water with respect to bulk water as a function of concentration, obtained from the fit of $\Psi^{TOT}(t)$ (pink symbols) and $\Psi^{W}(t)$ (cyan symbols) and from experiment (gray symbols).[26]

water contribution $\Psi^{W}(t)$ at all concentrations, giving a retardation ratio ξ similar to that obtained from $\Psi^{TOT}(t)$ (Figure 8), thus supporting the scenario in which two populations with different dynamics exist for water in sugar solutions and reinforcing the belief that water dynamics dominate EDLS at the ps time scales. The characteristic

dx.doi.org/10.1021/jp301988f | J. Phys. Chem. B 2012, 116, 7499–7508

relaxation times obtained for water are smaller than the residence times estimated for sugar aqueous solutions from the time integrals of the intermittent hydrogen bond time correlation functions between water and carbohydrate molecules.[22] This indicates that the slow exchange condition is satisfied and confirms the ability of OKE and DLS techniques to distinguish between the two water species.

Recently, self-intermediate scattering functions for water in aqueous trehalose solutions have been fitted with a similar procedure,[23] showing two distinct relaxation processes with characteristic relaxation times at room temperature very close to the ones obtained in the present work. Moreover, MD simulations of aqueous solutions of fructose[22] showed characteristic H-bond lifetimes for fructose-water bonds longer than the water−water lifetimes, and, in fairly dilute conditions, a retardation between the two relaxation times of less than an order of magnitude, closely resembling the retardation ratios reported here. These results support the observation (see Figure 4) that the characteristic relaxation probed through the relaxation of the collective polarizability is dominated by water translational dynamics and suggest its relaxation times to be closely related to the relaxation of the H-bond network in the mixture, similar to the mechanism found in simulations of OKE in aqueous solutions of formamide.[50]

Finally, let us stress the possibility to independently deriving from the calculated TCFs the average number of water molecules dynamically perturbed by the presence of a solute molecule from the amplitude of the relaxation processes of bulk Δ_{bulk} and hydration Δ_{hyd} water. The hydration numbers N_h obtained from the relationship

$$N_h = \frac{1}{f_r}\frac{\Delta_{hyd}}{(\Delta_{hyd} + \Delta_{bulk})} \quad (27)$$

where $f_r = N_{TRE}/N_W$ is the ratio of solute over water molecules, are reported in Figure 9 as resulting from $\Psi^{TOT}(t)$ and $\Psi^{W}(t)$.

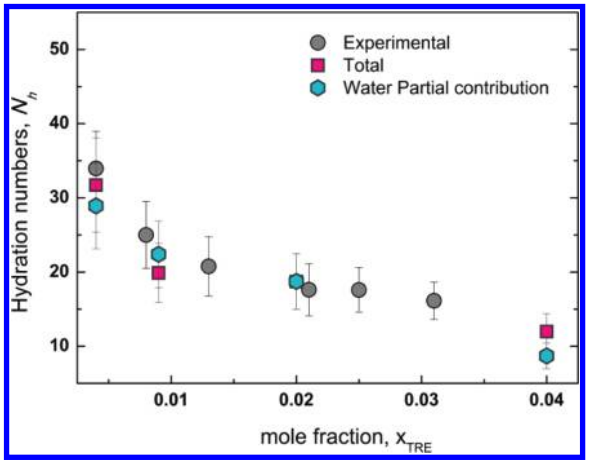

Figure 9. Hydration numbers as a function of trehalose concentration, obtained from the present analysis and from previous experimental results.[26]

Similar values are obtained, again comparable with the experimental ones (Figure 9).[26] In previous work[26] a hydration number of ca. 17, estimated by averaging data at different concentrations, was reported. According to MD results,[18,27,55] this number mainly accounts for the number of water molecules H-bonded to the solute. As can be seen from Figure 9, experimental and computational results agree in suggesting a decrease of hydration number with increasing trehalose mole fraction. This trend agrees with the concentration dependence of N_h found in previous MD simulations.[55] At the lowest trehalose concentration, for which the intensity of the hydration component is low, we used a modified fitting procedure to obtain N_h. Specifically, we required that the value of τ_{bulk} be approximately the same as for pure water. The reported dependence on solute concentration can be interpreted as being caused by the superposition of hydration shells and solute clustering, both of which increase with increasing trehalose concentration.[55] The extent of clustering at higher concentrations depends on solute hydrophilicity, as was shown in a recent simulation study.[56] Self-association of aqueous trehalose has recently been investigated[57] and the most probable coordination number for trehalose aqueous solutions, defined as the number of directly H-bonded trehalose molecules to any other trehalose molecule, has been found to remain lower than two in the concentration range of the present work, with an average lifetime for these aggregates of about 11 ps.[57] Comparison of MD simulation results for disaccharides indicates that trehalose molecules have a lower tendency toward clustering than do maltose[23,55] and fructose[55] molecules. Thus superposition of hydration shells is the more likely reason for decrease in N_h with increasing X_{TRE}.

As a whole, the results on hydration numbers show a dynamical perturbation that does not extend beyond the first hydration shell of the carbohydrate molecule, thus suggesting a moderate spatial perturbation imposed by trehalose on water. Water molecules closer to the trehalose interface, but not necessarily H-bonded to it, are slowed down more. As recently pointed out,[23] dynamical investigations cannot provide a direct assessment of the structure of the system, such as distortion or breaking of the hydrogen bond network of water due to strong interactions between water and trehalose, but can provide valuable information on the spatial extent of the dynamical perturbation and on the location of water molecules affected by it, using additional information accessible through analysis of MD data. Finally, it is important at this point to observe that depolarized light scattering measurement of lysozyme and an amphiphilic peptide,[32,33] showed larger retardation factors, suggesting a more local and moderate dynamical perturbation for solutions of carbohydrates than for peptide solutions.

IV. CONCLUSIONS

EDLS and OKE have been widely used[26,32−35,58] to investigate the dynamics of water in solutions of biological molecules of growing complexity. The experimental data in the ∼0.6−1000 GHz have been interpreted as the sum of three different relaxation processes assigned to the solute, and to hydration and bulk water molecules. The validity of this interpretation, which assumes a marked spectral separation of these contributions, was indirectly confirmed by two main pieces of evidence: the agreement between the temperature behavior of the relaxation times obtained from the bulk component and those measured for pure water and the result that the relaxation times obtained from the low-frequency component satisfy of the Stokes−Einstein−Debye relationship. The present work provides evidence for such a spectral separation, based on an independent MD investigation. In particular, the positive comparison between the relaxation times of bulk and hydration water obtained from the fit of total and water contribution, endorses the dynamical scenario in which the frequency region

above ∼10 GHz is dominated by water dynamics, while the similarity between hydration numbers calculated from total and water contributions ensures that not only the retardation factor, but also the number of water molecules slowed down by the presence of the solute molecules is well estimated by the analysis of the experimental data. Furthermore, a decrease of hydration numbers with increasing trehalose concentration has been found and can be simply explained as the superposition of hydration shells. The analysis presented here results in an overall greater number of perturbed solvent molecules per solute molecule, compared to the average value of 17, previously suggested as the number of water molecules hydrogen bonded to the solute.[26]

As a whole our results suggest that OKE and DLS techniques are suitable to probe the dynamics of water surrounding biological molecules, providing reliable information on the retardation ratio between hydration and bulk water molecules and the number of water molecules involved in the slowing down of relaxation. Issues such as the dynamical behavior of hydration water upon changing the chemical heterogeneity of solutes as well as upon supercooling can be conveniently approached.

AUTHOR INFORMATION

Corresponding Author

*E-mail: laura.lupi@fisica.unipg.it.

Notes

The authors declare no competing financial interest.

ACKNOWLEDGMENTS

B.M.L. gratefully acknowledges the U.S. National Science Foundation, Grant No. CHE-0911668, for partial support of this research.

REFERENCES

(1) Kropman, M. F.; Bakker, H. J. *Science* **2001**, *291*, 2118−2120.
(2) Pal, S. K.; Peon, J.; Zewail, A. H. *Proc. Natl. Acad. Sci. U.S.A* **2002**, *99*, 15297−15302.
(3) Bagchi, B. *Chem. Rev.* **2005**, *105*, 3197−3219.
(4) Miura, N.; Asaka, N.; Shinyashiki, N.; Mashimo, S. *Biopolymers* **1994**, *34*, 357−364.
(5) Halle, B.; Davidovic, M. *Proc. Natl. Acad. Sci. U.S.A.* **2003**, *100*, 12135−12140.
(6) Crowe, J. H.; Crowe, L. M.; Chapman, D. *Science* **1984**, *223*, 701−703.
(7) Carpenter, J. F.; Crowe, J. H. *Biochemistry* **1989**, *28*, 3916−3922.
(8) Crowe, J. H.; Crowe, L. M. *Nat. Biotechnol.* **2000**, *18*, 145−146.
(9) Cesaro, A. *Nat. Mater.* **2006**, *5*, 593−594.
(10) Ding, S. P.; Fan, J.; Green, J. L.; Lu, Q.; Sanchez, E.; Angell, C. A. *J. Therm. Anal.* **1996**, *47*, 1391−1405.
(11) Sussich, F.; Urbani, R.; Princivalle, F.; Cesaro, A. *J. Am. Chem. Soc.* **1998**, *120*, 7893−7899.
(12) Branca, C.; Magazu, S.; Maisano, G.; Migliardo, P. *J. Chem. Phys.* **1999**, *111*, 281−287.
(13) Villarreal, M. A.; Diaz, S. B.; Disalvo, E. A.; Montich, G. G. *Langmuir* **2004**, *20*, 7844−7851.
(14) Branca, C.; Magazu, S.; Maisano, G.; Migliardo, P. *J. Phys. Chem. B* **1999**, *103*, 1347−1353.
(15) Malsam, J.; Aksan, A. *J. Phys. Chem. B* **2009**, *113*, 6792−6799.
(16) Sakurai, M.; Murata, M.; Inoue, Y.; Hino, A.; Kobayashi, S. *Bull. Chem. Soc. Jpn.* **1997**, *70*, 847−858.
(17) Bonanno, G.; Noto, R.; Fornili, S. L. *J. Chem. Soc., Faraday Trans.* **1998**, *94*, 2755−2762.
(18) Lee, S. L.; Debenedetti, P. G.; Errington, J. R. *J. Chem. Phys.* **2005**, *122*, 204511.
(19) Heugen, U.; Schwaab, G.; Brundermann, E.; Heyden, M.; Yu, X.; Leitner, D. M.; Havenith, M. *Proc. Natl. Acad. Sci. U.S.A.* **2006**, *103*, 12301−12306.
(20) Heyden, M.; Brundermann, E.; Heugen, U.; Niehues, G.; Leitner, D. M.; Havenith, M. *J. Am. Chem. Soc.* **2008**, *130*, 5773−5779.
(21) Choi, Y.; Cho, K. W.; Jeong, K.; Jung, S. *Carbohydr. Res.* **2006**, *341*, 1020−1028.
(22) Sonoda, M. T.; Skaf, M. S. *J. Phys. Chem. B* **2007**, *111*, 11948−11956.
(23) Magno, A.; Gallo, P. *J. Phys. Chem. Lett.* **2011**, *2*, 977−982.
(24) Verde, A. V.; Campen, R. K. *J. Phys. Chem. B* **2011**, *115*, 7069−7084.
(25) Pomata, M. H. H.; Sonoda, M. T.; Skaf, M. S.; Elola, M. D. *J. Phys. Chem. B* **2009**, *113*, 12999−13006.
(26) Paolantoni, M.; Comez, L.; Gallina, M. E.; Sassi, P.; Scarponi, F.; Fioretto, D.; Morresi, A. *J. Phys. Chem. B* **2009**, *113*, 7874−7878.
(27) Liu, Q.; Schmidt, R. K.; Teo, B.; Karplus, P. A.; Brady, J. W. *J. Am. Chem. Soc.* **1997**, *119*, 7851−7862.
(28) Conrad, P. B.; de Pablo, J. J. *J. Phys. Chem. A* **1999**, *103*, 4049−4055.
(29) Fioretto, D.; Comez, L.; Gallina, M. E.; Morresi, A.; Palmieri, L.; Paolantoni, M.; Sassi, P.; Scarponi, F. *Chem. Phys. Lett.* **2007**, *441*, 232−236.
(30) Paolantoni, M.; Comez, L.; Fioretto, D.; Gallina, M. E.; Morresi, A.; Sassi, P.; Scarponi, F. *J. Raman Spectrosc.* **2008**, *39*, 238−243.
(31) Gallina, M. E.; Comez, L.; Morresi, A.; Paolantoni, M.; Perticaroli, S.; Sassi, P.; Fioretto, D. *J. Chem. Phys.* **2010**, *132*, 214508.
(32) Perticaroli, S.; Comez, L.; Paolantoni, M.; Sassi, P.; Morresi, A.; Fioretto, D. *J. Am. Chem. Soc.* **2011**, *133*, 12063−12068.
(33) Perticaroli, S.; Comez, L.; Paolantoni, M.; Sassi, P.; Lupi, L.; Fioretto, D.; Paciaroni, A.; Morresi, A. *J. Phys. Chem. B* **2010**, *114*, 8262−8269.
(34) Mazur, K.; Heisler, I. A.; Meech, S. R. *J. Phys. Chem. B* **2010**, *114*, 10684−10691.
(35) Mazur, K.; Heisler, I. A.; Meech, S. R. *J. Phys. Chem. B* **2011**, *115*, 2563−2573.
(36) Smith, W.; Forester, T. R. *DL_POLY 2*, CCLRC; Daresbury Laboratory: Daresbury, U.K.
(37) Smith, W.; Todorov, I. T. *Mol. Simul.* **2006**, *32*, 935−943.
(38) Berendsen, H. J. C.; Grigera, J. R.; Straatsma, T. P. *J. Phys. Chem.* **1987**, *91*, 6269−6271.
(39) Damm, W.; Frontera, A.; TiradoRives, J.; Jorgensen, W. L. *J. Comput. Chem.* **1997**, *18*, 1955−1970.
(40) Allen, M. P.; Tildesley, D. J., *Computer simulation of liquids*; Oxford University Press: New York, 1987.
(41) Ciccotti, G.; Ferrario, M.; Ryckaert, J. P. *Mol. Phys.* **1982**, *47*, 1253−1264.
(42) Geiger, L. C.; Ladanyi, B. M. *Chem. Phys. Lett.* **1989**, *159*, 413−420.
(43) Paolantoni, M.; Ladanyi, B. M. *J. Chem. Phys.* **2002**, *117*, 3856−3873.
(44) Skaf, M. S.; Vechi, S. M. *J. Chem. Phys.* **2003**, *119*, 2181−2187.
(45) Murphy, W. F. *J. Chem. Phys.* **1977**, *67*, 5877−5882.
(46) Skaf, M. S.; Sonoda, M. T. *Phys. Rev. Lett.* **2005**, *94*, 137802.
(47) Torre, R.; Bartolini, P.; Righini, R. *Nature* **2004**, *428*, 296−299.
(48) Thole, B. T. *Chem. Phys.* **1981**, *59*, 341−350.
(49) van Duijnen, P. T.; Swart, M. *J. Phys. Chem. A* **1998**, *102*, 2399−2407.
(50) Elola, M. D.; Ladanyi, B. M. *J. Chem. Phys.* **2007**, *126*, 084504.
(51) Paolantoni, M.; Sassi, P.; Morresi, A.; Santini, S. *J. Chem. Phys.* **2007**, *127*, 024504.
(52) Sonoda, M. T.; Vechi, S. M.; Skaf, M. S. *Phys. Chem. Chem. Phys.* **2005**, *7*, 1176−1180.
(53) Williams, G.; Watts, D. C. *Trans. Faraday Soc.* **1970**, *66*, 80−&.
(54) Sokolov, A. P.; Hurst, J.; Quitmann, D. *Phys. Rev. B* **1995**, *51*, 12865−12868.
(55) Lerbret, A.; Bordat, P.; Affouard, F.; Descamps, M.; Migliardo, F. *J. Phys. Chem. B* **2005**, *109*, 11046−11057.

(56) Stirnemann, G.; Sterpone, F.; Laage, D. *J. Phys. Chem. B* **2011**, *115*, 3254−3262.
(57) Sapir, L.; Harries, D. *J. Phys. Chem. B* **2011**, *115*, 624−634.
(58) Rossi, B.; Comez, L.; Fioretto, D.; Lupi, L.; Caponi, S.; Rossi, F. *J. Raman Spectrosc.* **2011**, *42*, 1479−1483.